

Article

Ligno-Cellulosic Fibre Sized with Nucleating Agents Promoting Transcristallinity in Isotactic Polypropylene Composites

Armin Thumm, Regis Risani, Alan Dickson^{ID} and Mathias Sorieul *

Scion, Forest Research Institute Ltd., 49 Sala street, 3020 Rotorua, New Zealand;
Armin.thumm@scionresearch.com (A.T.); Regis.risani@scionresearch.com (R.R.);
Alan.dickson@scionresearch.com (A.D.)

* Correspondence: Mathias.sorieul@scionresearch.com; Tel.: +64-7343-5514

Received: 20 February 2020; Accepted: 9 March 2020; Published: 10 March 2020



Abstract: The mechanical performance of composites made from isotactic polypropylene reinforced with natural fibres depends on the interface between fibre and matrix, as well as matrix crystallinity. Sizing the fibre surface with nucleating agents to promote transcristallinity is a potential route to improve the mechanical properties. The sizing of thermo-mechanical pulp and regenerated cellulose (Tencel™) fibres with α - and β -nucleating agents, to improve tensile strength and impact strength respectively, was assessed in this study. Polarised microscopy, electron microscopy and differential scanning calorimetry (DSC) showed that transcristallinity was achieved and that the bulk crystallinity of the matrix was affected during processing (compounding and injection moulding). However, despite substantial changes in crystal structure in the final composite, the sizing method used did not lead to significant changes regarding the overall composite mechanical performance.

Keywords: nucleating agent; isotactic polypropylene; transcristallinity; natural fibres; Tencel™

1. Introduction

Isotactic polypropylene (iPP) is an important engineering thermoplastic polyolefin used in many different commercial applications such as packaging and automotive parts [1]. The main advantages of iPP are its easy processing and low manufacturing cost [2]. Its mechanical behaviour, thermal properties, and chemical resistance depend on its semi-crystalline structure and fraction (typically 50%–70%) [3]. Isotactic polypropylene is a non-polar, polymorphic polymer. The three basic crystal forms of iPP are: the monoclinic alpha (α) form, the trigonal beta (β) form and the orthorhombic gamma (γ) form [4,5]. The α -form crystals are obtained under common processing conditions, between 60 °C and 188 °C, with a maximum crystallisation rate around 80 °C [6,7]. In composites, the presence of α -crystals improves thermodynamic stability and mechanical performance but also reduces the impact strength, especially at low temperature. The β -form crystals are metastable thermodynamically, and have several advantages over the α -form, such as improved elongation at break and improved impact strength [8,9]. The β -crystals fan-shaped morphology has the ability to dissipate the impact energy, therefore improving toughness [10]. The β -form can be obtained using a temperature gradient method [11], shear flow-induced crystallization [12,13] or specific nucleating agents (NA) [14]. A temperature of crystallisation around 130 °C is best to promote nucleation and growth of β -iPP crystals [15,16].

It is a common strategy to improve the mechanical properties of polyolefin-based materials via the introduction of reinforcing agents (e.g., carbon fibres, glass fibres, clays, lignocellulosic materials). The strength of composite materials is influenced by: matrix properties, intrinsic properties of

the reinforcement, dispersion of the reinforcement in the matrix, degree of orientation, quality of the interface and volume fraction of reinforcement [17,18]. In the resulting composite, the stress concentration develops at the interface between the matrix and reinforcement agent and is mainly influenced by the following: the volume fraction; the thermal expansion coefficient difference between each material; the interphase; and the crystallisation of the matrix. To achieve high mechanical performance, good interfacial adhesion allowing stress transfer between the matrix and reinforcement agent is crucial [19,20]. Several methods have been developed to improve interfacial adhesion between highly polar fibres and nonpolar polymers. The most common strategies used are sizing, compatibilisation, polymer grafting and interfacial crystallisation [10]. Transcristallinity (TC) or transcristalline layers describes a crystalline structure with limited thickness located at the interphase region, it originates from a high density of heterogeneous nuclei with a crystal growth orientation mainly perpendicular to the fibre surface until the growing front impinges with spherulites nucleated in the bulk [21,22]. The development of a TC structure is a promising route for improving the load transfer between the semi-crystalline matrix and the fibre [23].

TC enhances fibre–matrix adhesion, reduces stress concentration, creates a mechanical interlock and a protective layer around the fibres leading to an efficient stress transfer from the matrix across the interphase [24]. Good TC is obtained when the crystallisation parameters are more favourable to the TC formation compared to the crystallisation of spherulites in the bulk [25]. In composites, the development of the TC layer is influenced by factors such as matrix type, thermal history, temperature of polymer crystallisation, chain mobility, rate of cooling, occurrence of shearing forces during crystallisation and thermal expansion coefficients of individual components [24,26]. The surface topology, composition and sizing of the fibre itself are major parameters influencing the TC formation [27]. To achieve good TC, high nucleation site density along the fibre surface is crucial [28]. The proximity of nucleation sites restricts the crystal growth to the lateral direction, leading to the development of a columnar layer around fibres [22,29].

Lignocellulosic fibres have many beneficial features such as biodegradability, renewability, availability, low cost, and ease of preparation [30]. Polymer composites incorporating lignocellulosic fibres offer several advantages including low density, good mechanical properties and high damping capabilities [31,32]. The lignocellulosic fibres chosen for this study were High Temperature Thermo-Mechanical Pulp fibres (HT TMP) and Tencel™. The HT TMP fibres are naturally coated with a thin, relatively non-polar, lignin layer [33–35]. Softwood HT TMP fibres are of industrial relevance due to their low cost of production and low weight advantage when compounded into plastic composites [36,37]. Tencel™ is a regenerated cellulose fibre which exhibits high tensile properties (strength of 1.4 GPa and modulus 36 GPa) [38] and was included in this study as a reference fibre, as its high ductility improves the impact characteristics of brittle polymer matrices [39].

This study investigates the potential of α - or β -nucleating agent (NA) as a sizing additive for improving the mechanical properties of an iPP-natural fibre composite. The hypothesis is that the NA will generate a high nucleation density on the fibre surface leading to an α or β specific TC, improving both tensile properties and/or impact resistance. The addition of the NA usually occurs at the compounding stage of composite manufacture. In this study, we developed an original approach by directly adding the NA onto the fibres that could be adopted to tailor the lignocellulosic fibre composite characteristics eliminating the need for the addition of NA at the compounding stage. Our novel approach was to coat the fibres with the NA prior to compounding with the iPP to create a TC structure with improved matrix-fibre stress transfer.

2. Materials and Methods

2.1. Materials

2.1.1. Fibres

Wood chips (*Pinus radiata*), were thermomechanically pulped at 180 °C at Scion's fibre and pulp processing pilot plant (Rotorua, New Zealand). The resulting HT TMP fibres were dried in a tube drier to approximately 12% moisture content. An earlier study has found that chips processed in this way lead to fibres with a cellulose content of 39%–42%, lignin content of 28%–31% and 22%–25% hemicelluloses [40]. Prior to processing the fibres were approximately 1.25 mm long and 0.03 mm wide. The length and aspect ratio were significantly reduced during compounding [41]. Tencel™ fibres were purchased from Lenzing Fibers GmbH (Heiligenkreuz, Austria).

2.1.2. Nucleating Agents

The α -NA was Hyperform® HPN-68L (Milliken Chemical, Blacksburg, SC, USA) and the β -NA was NU-100 (NJStar), (New Japan Chemical Co. Ltd., Osaka, Japan). Hyperform® HPN-68L is a powdered α -NA comprising a dicarboxylate sodium-based compound known as HPN-68L. It is used to reduce cycle time and improve the tensile and flexural mechanical properties of the iPP [42]. Nu-100 (NJSTAR NU-100) is a β -NA. Its active ingredient, N,N'-dicyclohexyl-2,6-naphthalenedicarboxamide (DCNDCA), has been found to be an effective β -NA [15]. However, DCNDCA is dual selective and can induce both α -phase and β -phase, depending on the thermal condition applied [15].

2.1.3. Polypropylene and Compatibiliser

Isotactic homo-polypropylene SJ-170, Hopelen was sourced from Lotte Chemical Co., Seosan, South Korea. The compatibiliser was 3% w/w maleic anhydride grafted polypropylene (MAPP) Epolene G3015 (Eastman Chemical Co., Kingsport, TN, USA). A 3% MAPP loading was used according to the manufacturer recommendation for 30% wt lignocellulosic fibre content.

2.2. Methods

2.2.1. Sizing of the Fibre and Fibre Pellet Production

Fibres were blended with an adhesive thermoplastic acrylated emulsion [36] and NA in a dry blender consisting of a 12 m steel loop (\varnothing : 0.15 m) with a fan that creates a turbulent flow. The adhesive was administered onto the fibre in the loop via an inserted spray gun. The NA powder was then slowly added into the loop and the materials were circulated in the loop for a further 2 min. The adhesive was added at a 4% wt loading with respect to oven-dried fibre. The NA was added at a 1.7% loading with respect to fibre (0.5% wt loading with respect to the finished composite). Coated fibres were hot-pressed into 3 mm thin sheets and subsequently cut into small dice (4 × 4 mm) with a pneumatic chopper. The process is described in detail in Warnes et al., [36].

2.2.2. Nitrogen Analysis

Between 0.25 and 0.5 g of fibre dice were heated in a stream of high purity oxygen in a Leco furnace (Laboratory Equipment Corporation, St Joseph, MI, USA) to produce CO₂, N₂ and NO_x. A subsample of the combustion gases was passed through a heated copper catalyst that further reduced the NO_x to N₂, which was then measured by thermal conductivity. This results in the percentage of total nitrogen. This percentage was converted to NA content of the final sample by subtracting the N content of a NA free reference from the sample containing NA and then dividing the resulting difference by the nitrogen content of the pure NA. This method could only be applied to the β -NA as the α -NA does not contain nitrogen.

2.2.3. Compounding

The HT TMP fibre dice and the TencelTM fibre dice were compounded at 30% wt loading into iPP with 3% wt maleic anhydride PP (MAPP) as a coupling agent. The LabTechTM extruder (LTE26-40, LabTech Engineering Co. Ltd., Samut Prakan, Thailand) had a 26 mm screw diameter, with co-rotating twin screws, with a 40 L/D (length/diameter) ratio. The PP and MAPP were dry blended and fed into the main feed throat using a WeighbatchTM DS20 (Weighbatch, Hamilton, New Zealand) gravimetric feeder. The fibre dice, which were oven dried overnight at 105 °C, were side-fed into the extruder using a K-Tron twin-screw gravimetric feeder (Coperion K-Tron, Sewell, NJ, USA). For the “no fibre” reference, the NAs were dry-blended with the iPP at the same time as the MAPP. Two atmospheric venting ports and one crammer vacuum (0.7 bar) degassing port were used to remove the entrapped air in the melt along with volatile organic compounds (VOCs). The melt was extruded through a 2-strand die and pulled into a water bath before being granulated into 3 mm long pellets. Each formulation was compounded in a single extrusion run at 200 rpm screw speed and 8 kg h⁻¹ total extrusion throughput to ensure proper fibre mixing with a gentle screw design and reverse barrel temperature profile (220 °C to 190 °C).

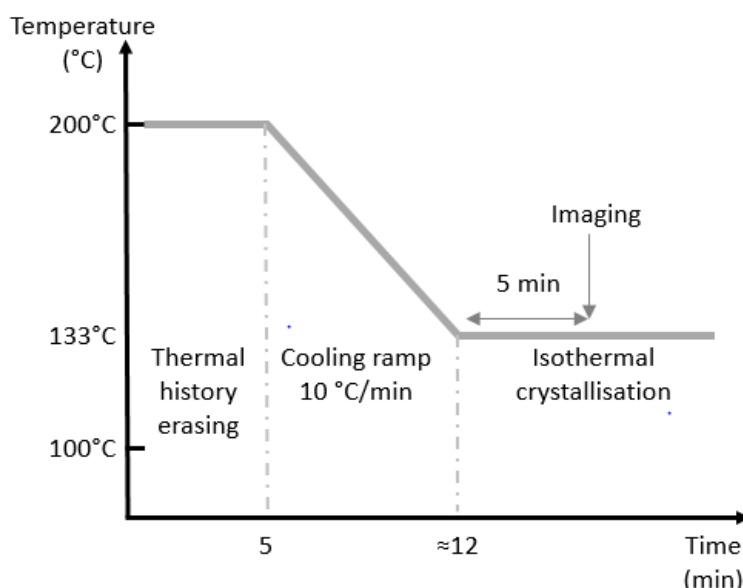
2.2.4. Injection Moulding

Prior to injection moulding, the compounded pellets were oven dried at 105 °C, to obtain a pellet with residual moisture content below 0.3% wt. The compounded pellets were injection moulded with a BOY 35 machine (BOY Spritzgiessautomaten, Neustadt-Fernthal, Neustadt-Fernthal, Germany) into ISO multipurpose injection moulded test specimens (dogbone) type A (ISO 3167). The barrel temperature of the injection moulder was 190 °C and the mould was kept at 30 °C. The injection speed was 100 mm s⁻¹. The mould was filled with a screw speed of 100 rpm with 15 bar back pressure. Cooling time was 20 s. The injection moulding parameters were the same for all composites. Injection moulded parts were collected once their weight was constant. Thirty test specimens were collected for each treatment with the first ten disregarded for analysis.

2.2.5. Polarised Light Optical Microscopy (PLOM)

Cross-polarized optical microscopy was performed with a Leica DMRB microscope (Leica Mikroskopie & Systeme GmbH, Wetzlar, Germany), using a Leica EC3 camera (Leica Microsystems Ltd., Singapore) and a 10× magnification lens (Leica PL Fluotar). The temperature was controlled during the experiments with a programmable Mettler-Toledo hot stage HS82 (Mettler-Toledo GmbH, Greifensee, Switzerland).

For each experiment, a piece of iPP thin film was placed on a glass microscopy slide. Individual fibres are then positioned onto the film. The slide was placed into the temperature-controlled stage [43]. The stage temperature was raised to 200 °C and once the iPP was molten, the sample was covered with a cover slip. After a 5-min holding period at 200 °C, to erase the thermal history of the sample, the temperature was decreased with a 10 °C/min ramp and stabilized at 133 °C to monitor the isothermal crystallisation (Scheme 1). The samples were imaged after 5 min of isothermal crystallisation at 133 °C. The temperature of 133 °C was chosen as it is the optimal temperature to promote β over α crystallisation [16,25].



Scheme 1. Schematic representation of thermal protocol applied on the Isotactic polypropylene (iPP)/fibre samples during polarised light optical microscopy (PLOM) measurements.

2.2.6. Etching

Injection moulded samples were etched based on the method of Olley [44]. This method removes any amorphous material so that the remaining crystalline structure could be observed by electron microscopy. A 35 mm section was cut from the middle part of a tensile specimen. The section was gently stirred for 6 h in a solution of 1.3% wt potassium permanganate (KMnO_4), 32.9% wt concentrated sulfuric acid (H_2SO_4) and 65.8% wt concentrated phosphoric acid (H_3PO_4) at room temperature. It was then cleaned with hydrogen peroxide for 5 min, rinsed with water, and dried overnight in an oven at 105 °C.

2.2.7. Scanning Electron Microscopy (SEM)

All SEM samples were coated with chromium using an Emitech K575X sputter coater (Quorum Technologies Ltd., Kent, UK) and imaged using a JEOL JSM 6700F (JEOL Ltd., Tokyo, Japan) at 3 kV accelerating voltage. For publication purposes the images were contrast enhanced using the enhanced local contrast (CLAHE) plugin in the ‘Fiji’ distribution of ImageJ (V1.5h) [45].

2.2.8. Crystal Size Measurement

The SEM images generated from the etched samples were analysed using V++ software (Digital Optics, Version 5.0, Wellington, New Zealand) to determine the diameter of the crystals. Approximately 50 crystals were measured for each treatment.

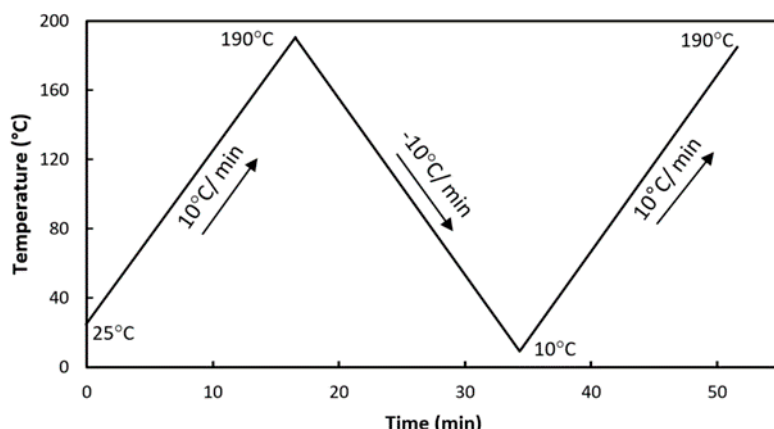
2.2.9. Differential Scanning Calorimetry (DSC)

For DSC analysis, all measurements were performed in triplicate. A transverse section (0.35 mm) was cut from the middle part of a tensile specimen. To avoid measuring the crystallinity of the skin of the test specimens, only the core of the transverse section (~5 mg) was used. All the calorimetric experiments were performed with a Discovery (TA instruments, USA) differential scanning calorimeter under nitrogen atmosphere (50 mL min^{-1}). The temperature scale was calibrated using indium, lead and tin as standards to ensure reliability of the data obtained. Melting temperatures, enthalpies, crystallisation and fusion peaks were determined by TRIOS software (TA Instruments, USA). The degree of crystallinity (X_c) was estimated using Equation (1) where ΔH_m is the measured melting enthalpy

of the polymeric part of the sample, W_f the fibre weight fraction in the composite, and $\Delta H_{100\%}$ the equilibrium melting enthalpy of 100% crystalline PP assumed to be 207 J g^{-1} [46].

$$X_c = 100 \times \frac{\Delta H_m}{\Delta H_{100\%}(1 - W_f)} \quad (1)$$

The thermal gradient of the DSC measurements is described in Scheme 2.



Scheme 2. Schematic illustration of the thermal protocol of the differential scanning calorimetry (DSC) measurements.

The enthalpy variations of the polymer during the initial heating ramp (Scheme 2), gives an indication of the thermal history related to the injection moulding conditions. A maximum temperature of 190°C was used to limit the natural fibre degradation but, as a consequence, the thermal history might not have been totally erased. This step is followed by a slow cooling ramp at a rate that favours the formation of a high β -fraction [15]. The melting cycle observed during the second heating ramp illustrates the crystal formation process which occurred during a controlled slow cooling with limited thermal history.

2.2.10. Mechanical Testing

Tensile and Modulus Tests

Tensile properties were measured on an Instron 5566 (Instron, Norwood, MA, USA) universal testing machine fitted with a 10 kN load cell and an external extensometer, according to ISO 527. The crosshead speed was 5 mm min^{-1} . The gauge length was 115 mm and the extensometer length were set to 25 mm. Ten specimens were tested to failure to obtain the average Young's modulus and maximum tensile stress.

Impact Test

Samples for Izod notched impact strength were prepared and tested in accordance with ASTM D 256. Samples were of dimensions $12.6 \text{ mm} \times 63.5 \text{ mm} \times \text{thickness}$ and a 45° notch was machined into each sample using a Ceast Notchvis (Ceast, Italy). Seven Izod samples for each variable were tested at a velocity of 3.46 m s^{-1} , a 150° angle and a 0.5 J hammer using a Ceast Resil impact testing machine (Ceast, Torino, Italy). Pull-out surfaces were compared between different formulations with SEM pictures taken from the central part of the transverse fracture area.

2.2.11. Water Uptake

ISO test specimens (dogbone) were submerged in water at 20°C for 70 days. During this time water uptake was monitored by briefly removing the samples from the water bath, wiping the surface

dry with a tissue and weighing them. This approach is based on ASTM D1037. Samples were measured in triplicate.

3. Results

3.1. Crystal Structure

The PLOM analysis showed no obvious transcrystallinity around the fibres without NA (Figure 1A,D). Although transcrystallisation is generally expected in cellulose fibres [47–50], it is also known to be impeded by the presence of lignin and hemicelluloses that decrease the frequency of nucleation sites and degree of crystallinity [51,52]. The absence of transcrystallinity with the untreated Tencel™ fibres is likely due to the cellulose II configuration of these artificially produced fibres which reduces nucleation activity [53–56].

Treatment with NA resulted in crystal growth perpendicular to the two types of fibres (Figure 1B,C and Figure 1E,F). The fibres treated with the β -NA (Figure 1C,F) showed better definition of the crystalline structure than those treated with the α -NA (Figure 1B,E).

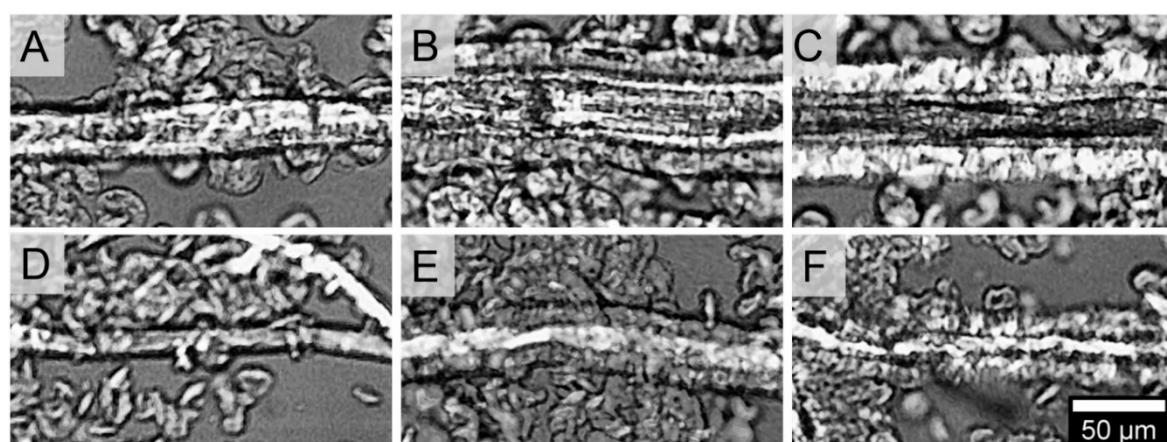


Figure 1. Optical micrographs of iPP trans-crystallisation around High Temperature Thermo-Mechanical Pulp fibres (HT TMP) and Tencel™ fibres with different sizing. The images are taken after a cooling period ($10\text{ }^{\circ}\text{C min}^{-1}$ ramp) and 5 min of isothermal crystallisation at $133\text{ }^{\circ}\text{C}$. (A) HT TMP only, (B) HT TMP + α -NA, (C) HT TMP + β -NA, (D) Tencel™ only, (E) Tencel™ + α -NA, (F) Tencel™ + β -NA. Scale bar = $50\text{ }\mu\text{m}$.

SEM of the composites after compounding and injection moulding confirmed that the iPP matrix containing fibres treated with the β -NA had iPP crystals that were fan-shaped, typical of β -crystals, whereas the samples without β -NA only showed α -crystal morphology (Figure 2). The etching process not only removes the amorphous phase of PP but also the fibres from the composite. The images show that the crystals were not specifically present around the space previously occupied by the fibre but seemed to be distributed throughout the matrix.

Compared to the controlled PLOM analysis, the compounded and injection moulded composites investigated by SEM were subjected to shear stresses and faster cooling. Large α -crystals were evident in the pure iPP (Figure 2a). The introduction of HT-TMP (Figure 2d) and Tencel™ (Figure 2g) fibres did not change the crystal type and morphology but their size was decreased by half (Figure 2j). This was the result of steric hindrance as the presence of the fibres increased the number of nucleation sites thereby increasing the crystal density and thus restricting the growth of the α -crystals. The α -NA resulted in a 30-fold size reduction of the α -crystals. This is likely due to the high number of nucleation sites leading to a growth competition. The addition of both types of fibres (Figure 2e,h) did not lead to further reduction of the crystal size (Figure 2j). The fan shaped β -crystals induced by the β -NA (Figure 2c) had an average diameter around $3.3\text{ }\mu\text{m}$ (Figure 2j). The addition of HT TMP and Tencel™

fibres (Figure 2c,f) also did not reduce the size of β -crystals further (Figure 2j). The hollows in the centre of β -spherulites are attributable to the etched DCNDCA particles [57].

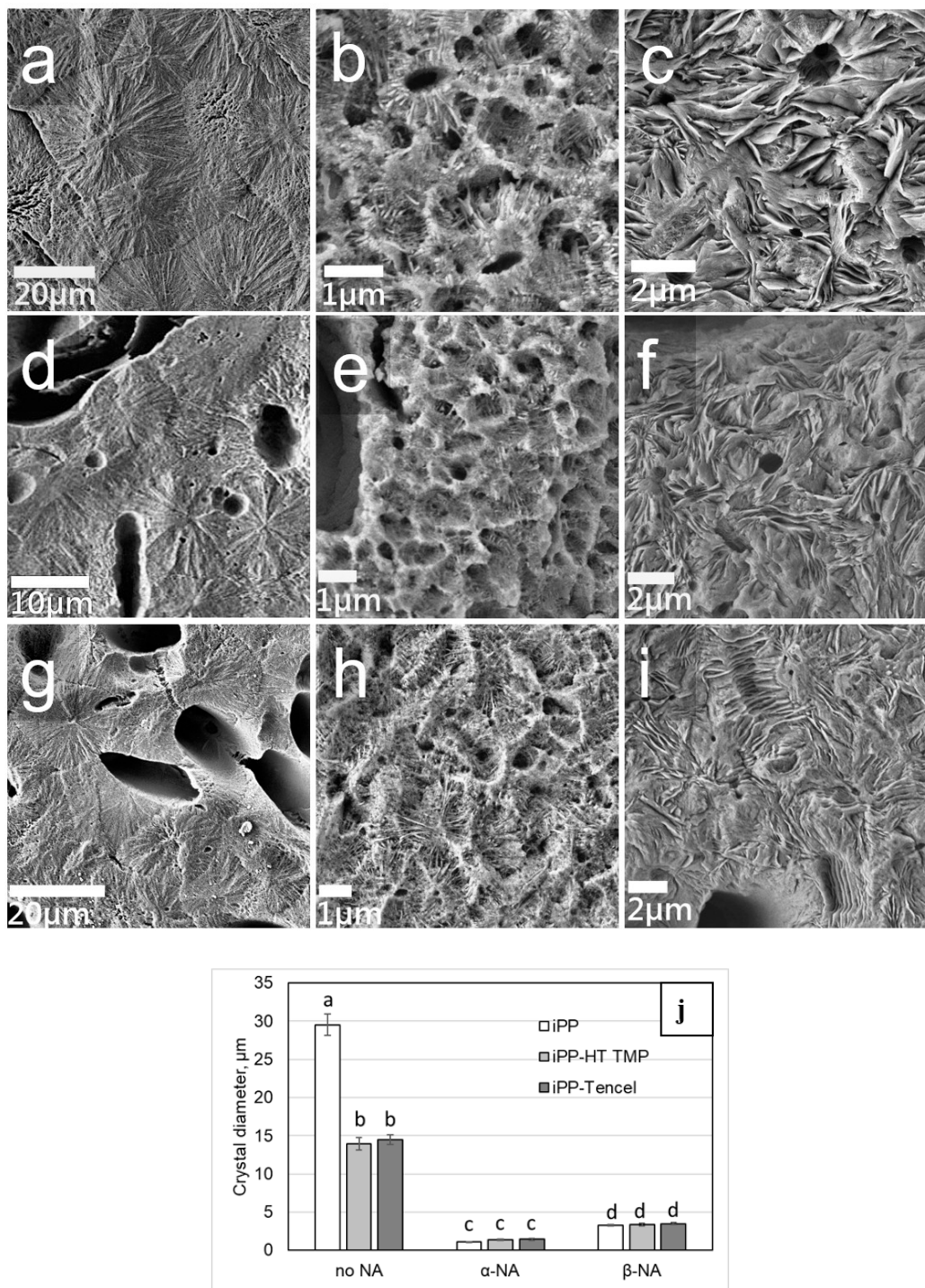


Figure 2. Scanning electron microscopy (SEM) images of iPP crystallisation. Transverse face of injection moulded samples after permanganate etching. (a) iPP, (b) iPP + α NA, (c) iPP + β -NA, (d) iPP + HT TMP, (e) iPP + HT TMP/ α -NA, (f) iPP + HT TMP/ β -NA, (g) iPP + TencelTM, (h) iPP+ TencelTM/ α -NA, (i) iPP + TencelTM + β -NA. (j) Crystal diameters of iPP and iPP composites with various NAs ($n \sim 60$, different letters indicate significant difference at $\alpha = 0.05$).

3.2. Differential Scanning Calorimetry (DSC)

Total crystallinity for all samples ranged between 36% and 45% (Table 1). The addition of fibre to the iPP had little effect on the overall crystallinity of the composites. The addition of NA also had little effect on the overall crystallinity of the iPP, however, the type of NA had a significant effect of the type of crystal structure present. As expected, no β -crystals were observed in the composites without the addition of β -NA.

The addition of β -NA, in the absence of fibre, led to an approximately 13% reduction of α -crystal enthalpy. The decrease in the proportion of α -crystals was compensated by the appearance of β -crystals. Therefore, the overall crystallinity was maintained. The same trend was observed in the presence of both types of fibre. Removal of the thermal history led to a larger decrease in α -crystals, down to ~10.5% and the highest level of β -crystals observed 34% and 30.4% for HT TMP and TencelTM, respectively. The presence of fibres coupled with a slow cooling ramp and without shear stress was the most favourable condition observed to generate a high β -crystal proportion. Our results are in accordance with Kang et al., who found that iPP in the presence of the dual selective β -NA (TMB-5) coupled and a slow cooling rate favoured the formation of high β -crystal fraction [15]. However, those results contradict Dong et al., [57] who found that fast cooling is favourable for creating high β -content in iPP/TMB-5 system. In our case, the slow cooling was favourable to the growth of β -crystals, possibly because the β -crystals formed at a higher temperature compared to α -crystals and, therefore, β -crystals had time to grow without competition from the α -crystals.

Evaluating how a combination of a slow cooling ramp and high shear stress (injection moulding) affects β -crystals formation was not technically possible. Indeed, fast cooling of the polymer is central to the injection moulding process to reduce cycle time without compromising on part quality [58].

The potential factors explaining why the composites containing HT TMP fibres had a higher β -crystals content compared to one with TencelTM fibres are probably related to the fibre surface. TencelTM fibres have a smooth surface [59] and HT TMP fibres are rough with a coating of lignin. A rough surface increases the interfacial shear strength [60] which is a factor favouring β -interfacial structures [61]. Moreover, lignin particles can increase β -crystallinity [62].

The addition of fibre into iPP without NA did not have a major influence on the melting temperature of the polymer, neither did the addition of the α -NA (Table 1). The melting temperature was around 163 °C for the α -crystals for all composites. The addition of the β -NA added a second melting peak at 152 °C (after removal of thermal history). For the samples with β -NA, the cooling process slightly shifts the β -crystals melting peaks.

Table 1. Comparison of α and β -crystal proportions and effect of α - and β -nucleating agent (NA) on iPP melting properties, after injection moulding or after melting and a slow cooling ramp (10 °C/min).

Fibre Type	Treatment	No NA		α -NA		β -NA		
		α	β	α	β	α	β	avg ($\alpha+\beta$)
HT TMP	After IM	36.4 ± 0.3	-	39.1 ± 2.1	-	23.0 ± 1.0	16.5 ± 0.5	39.5
	Slow ramp	39.8 ± 1.9	-	45.1 ± 1.8	-	27.0 ± 1.5	15.5 ± 1.2	42.5
	After IM	41.6 ± 0.4	-	35.8 ± 3.7	-	23.8 ± 1.0	15.5 ± 0.1	39.3
	Slow ramp	42.1 ± 1.5	-	41.8 ± 0.5	-	11.1 ± 0.9	34.0 ± 1.1	45.1
Tencel TM	After IM	42.0 ± 2.7	-	36.0 ± 3.4	-	28.5 ± 2.8	12.7 ± 1.0	41.2
	Slow ramp	38.1 ± 0.5	-	37.8 ± 1.8	-	10.1 ± 0.6	30.4 ± 0.9	40.5
Melting Peak Temperature (°C)								
HT TMP	After IM	166.4 ± 0.3	-	163.0 ± 0.2	-	163.9 ± 0.3	148.9 ± 0.3	
	Slow ramp	163.1 ± 0.2	-	164.1 ± 0.1	-	163.5 ± 0.2	151.5 ± 0.2	
	After IM	164.8 ± 0.7	-	163.3 ± 0.2	-	163.7 ± 0.1	146.6 ± 0.0	
	Slow ramp	161.9 ± 0.2	-	165.0 ± 0.1	-	163.1 ± 0.1	151.7 ± 0.1	
Tencel TM	After IM	163.9 ± 0.5	-	161.8 ± 0.2	-	164.3 ± 0.3	147.4 ± 0.2	
	Slow ramp	162.2 ± 0.3	-	163.7 ± 0.2	-	164.4 ± 0.9	152.3 ± 0.0	

Compared to IM, after a 10 °C min⁻¹ cooling ramp, the melting peak temperature of the β -crystals increases by 2.6 °C, 5.1 °C and 4.9 °C for the iPP with β -NA without fibres, with HT TMP and with

Tencel™ respectively. This indicates that the β -crystals which were grown at high temperature during slow cooling are more stable and therefore melt at higher temperature [63].

Samples were cut from the centre of the transverse surface of a tensile test specimen (dogbone). Proportions are extracted from integration of the melting peaks obtained from the DSC experiment. ($n = 3, \pm$ = standard deviation)

For industrial processing, the crystallisation temperature is an important parameter as a higher crystallisation temperature allows faster processing [64]. The presence of fibre in the iPP increases nucleation sites, and thus the crystallisation temperature by 6 and 8 °C for the HT TMP and the Tencel™, respectively (Figure 3).

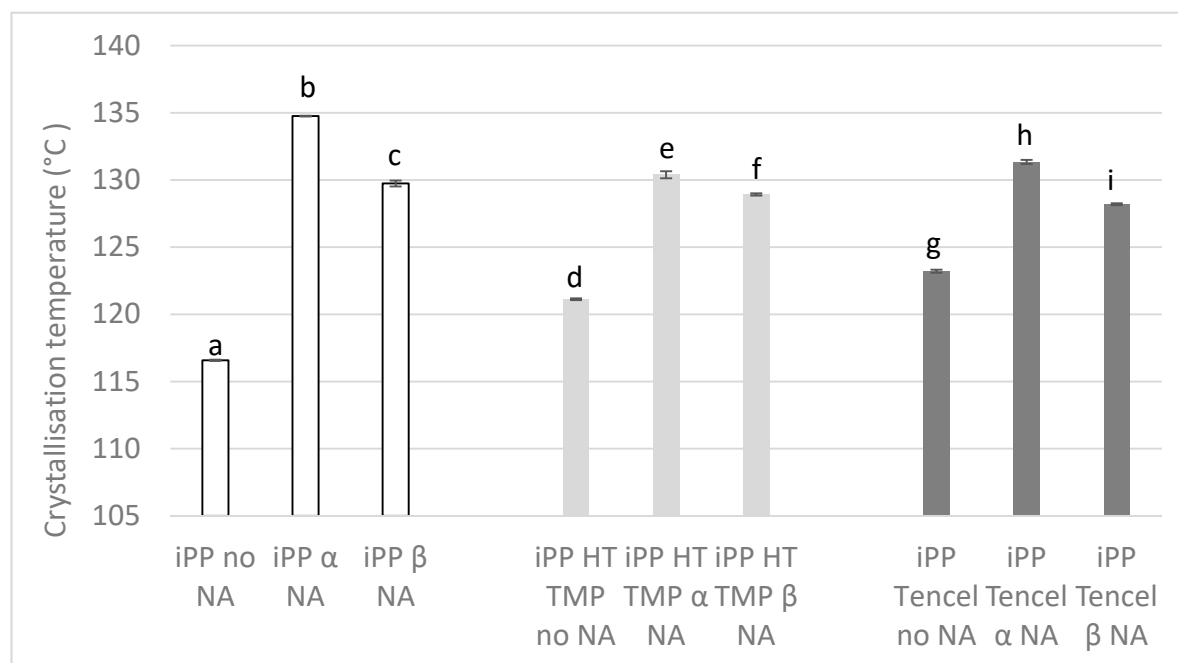


Figure 3. Effect of NA and fibres on iPP crystallisation temperature during a 10 °C min^{−1} cooling ramp ($n = 3$, different letters indicate significant difference at $\alpha = 0.05$).

Addition of α -NA does not affect the proportion of α -crystals in the iPP, but its crystallisation temperature is 20 °C higher. This is lowered with the addition of fibre. In presence of α -NA, the crystallisation temperature for HT TMP and Tencel™ composites increased by 12 and 8 °C, respectively. The addition of β -NA leads to a 15 °C rise in crystallisation temperature for the pure iPP. Again, this was lowered with the addition of fibre. The presence of β -NA lead to 8 and 5 °C increase in crystallisation temperature for the HT TMP and Tencel™ iPP composites, respectively. Overall, the pattern of crystallisation temperature increase remains the same for composites filled with either fibre, with a minor antagonist effect when the NA and fibres are present together.

3.3. Mechanical Properties

For commercial application, obtaining a composite with good mechanical properties especially yield strength and impact strength is extremely important [58].

3.3.1. Young's Modulus and Stress

The addition of fibre to iPP led to at least a doubling of the Young's Modulus (Figure 4a). The effect of the NA alone is minimal in comparison, with an increase of 29% and 17% for α -NA and β -NA added to iPP. Additionally, the addition of both NAs in presence of fibres has no significant effect on Young's Modulus of the composites with the exception of α -NA with Tencel™ (+18%).

The situation is relatively similar for tensile maximum stress properties (Figure 4b). The addition of β -NA has no effect on iPP, while the α -NA leads to a moderate increase (+13%). The addition of HT TMP and Tencel™ generates an increase in tensile maximum stress of 46% and 75%, respectively. In all cases, the addition of α -NA lead to a minor increase, while the β -NA lead to an expected small decrease in tensile maximum stress.

3.3.2. Impact Strength

Reinforcing iPP with HT TMP fibre gave an improvement in impact strength of the composite (Figure 4c). Adding an impact strength modifier, such as a β -NA, to the fibre was considered an opportunity to further enhance impact performance. Compared to pure iPP, the sole addition of HT TMP fibre led to a 46% increase in impact strength. When added in conjunction with HT TMP fibre, the α -NA addition reduces the impact strength of the fibre composite compared to the addition of fibre alone. β -NA has no significant influence. The major gain is due to the presence of HT TMP. A major improvement in impact strength comes from the addition of Tencel™ fibres with an increase of 181%. Addition of α -NA led to no significant change, while the addition of the β -NA led to moderate further improvement (+17%).

In summary, the main improvement for mechanical properties comes from the presence of the fibres themselves. In some cases, the NAs are providing a further minor improvement but in other cases, they can also have detrimental effects.

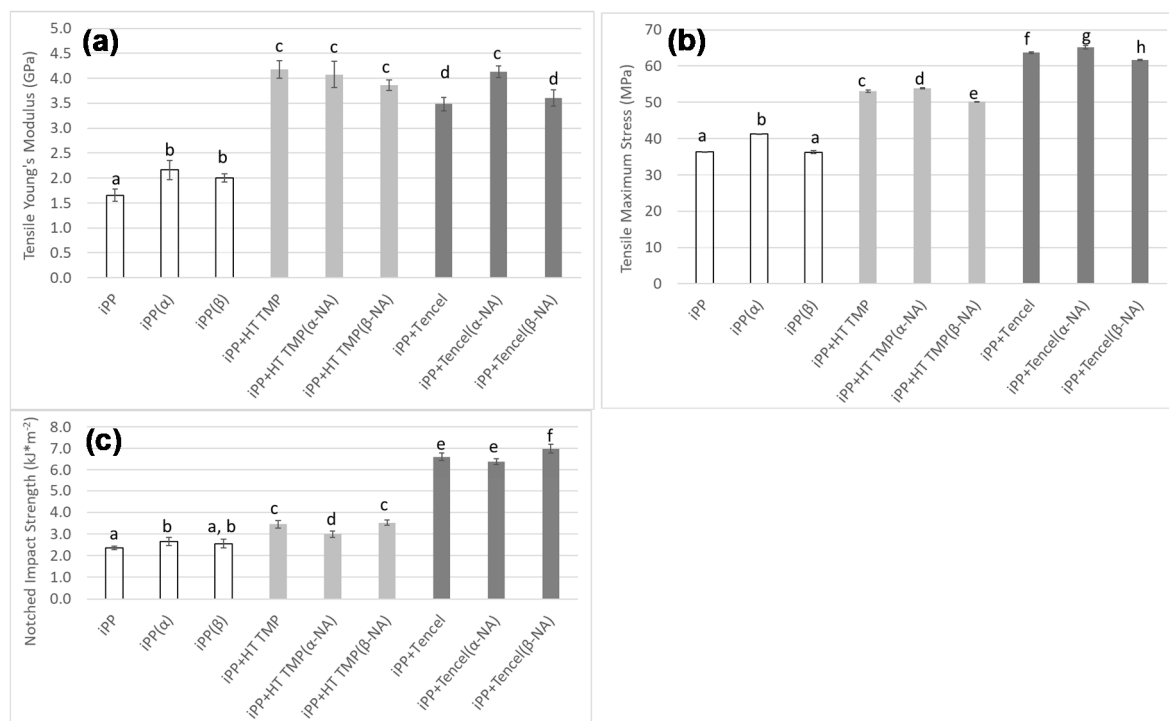


Figure 4. Influence of the α - and β -NA and HT TMP and Tencel™ fibres on (a) Young's modulus, (b) tensile maximum stress, and (c) notched impact strength. (Anova: different letter indicates significant difference at $\alpha = 0.05$).

3.4. Pull Out

SEM micrographs of transverse fracture surfaces from tensile testing samples show only minor pull-out of fibres for HT TMP filled composites (Figure 5). The few visible fibres appear to be delaminated or covered in matrix. The influence of lignin is complex, although lignin removal was found to improve composite properties [65], the presence of lignin can also have the effect of improving properties due to its interaction with coupling agents [66–69]. There are no visually observable

differences in pull-out between the different HT TMP treatments. The fracture surfaces of TencelTM filled-composites show a large number of fibres being pulled-out across all treatments. No matrix material adheres to the pulled-out fibres. It indicates that the interfacial adhesion between TencelTM and iPP is either lower than that of HT TMP and iPP or it can be explained by their higher shear strength compared to the HT TMP fibre [70,71]. Those observations agree with the higher impact strength observed for the Tencel-based composites, as a composite containing high strength fibres weakly compatibilized with the matrix will exhibit good impact performance. The TC layer observed by PLOM in the sandwich composite is clearly not covalently attached to the TencelTM fibres after injection moulding. The NA do not seem to have a strong effect on the interface.

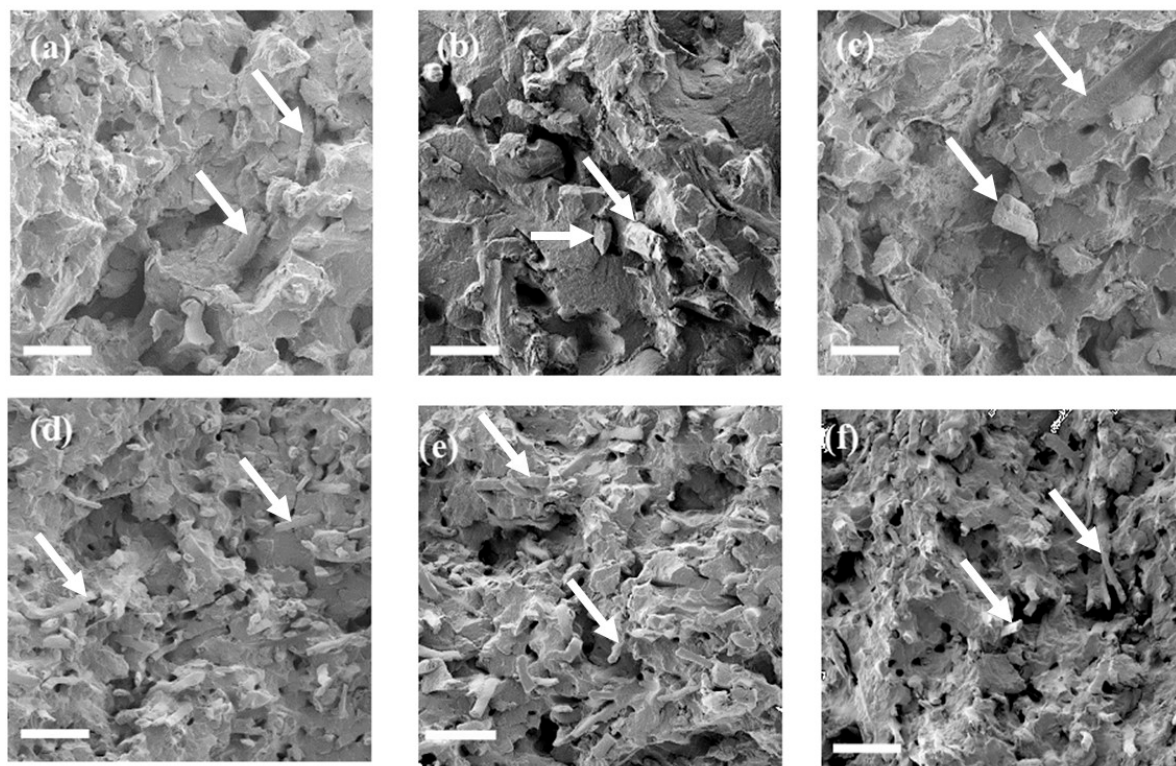


Figure 5. Comparison of pull-out surface between HT TMP and Tencel, from SEM pictures of transverse tensile test specimen fracture area. (a) HT TMP only, (b) HT TMP + α -NA, (c) HT TMP + β -NA, (d) TencelTM only, (e) TencelTM + α -NA, (f) TencelTM + β -NA. Arrows indicate fibres. Scale bar = 100 μ m.

3.5. Water Uptake

A slow water absorption rate allows for better dimensional stability of the composite when exposed to humidity. The nine formulations were immersed in water for 70 days. The results are expressed in percentage of water absorbed (Figure 6 and Table 2). The water uptake of the pure hydrophobic iPP is relatively low (0.3%). This value is comparable to previous studies [72]. The addition of β -NA leads to a slight but significant decrease in water absorption.

The hydrophilic character of natural fibres, ascribed to the bonding of water molecules to the free hydroxyl group is responsible for a water uptake increase in the plastic-fibre composites [73]. The addition of HT TMP and TencelTM to iPP lead to an increase of water absorption to around 2%. This indicates that the two types of fibres have the same type of hydrophilic behaviour. Surface treatment of fibre has often been used to decrease natural fibre composite water uptake [74,75]. Wu et al., [76] compared the water absorption of flax fibres functionalised with MAPP within either α or β crystalline iPP matrix. They did not observe any difference between the two types of crystal matrix. However, when the fibres were not functionalised, the α matrix containing the flax fibres had a slightly

higher water absorption than its β crystals counterpart. In our case, the addition of β -NA similarly shows a small but significant reduction in water uptake that is consistent across all treatments.

Unexpectedly, the addition of α -NA shows a significant increase in water uptake for samples containing fibres. The increase is only 0.5% in the case of the slightly hydrophobic HT TMP fibres, but is more pronounced (3.4%) in the case of the hydrophilic TencelTM fibres.

Additionally, DSC analysis (shown earlier) indicated the crystallinity of the α -NA and fibre composites was lower than both the control and β -NA composites which is correlated to this increase in water uptake. This increase in amorphous structure will create pathways for accelerating the water penetration into the composite. The larger the decrease in crystallinity, the larger the water uptake

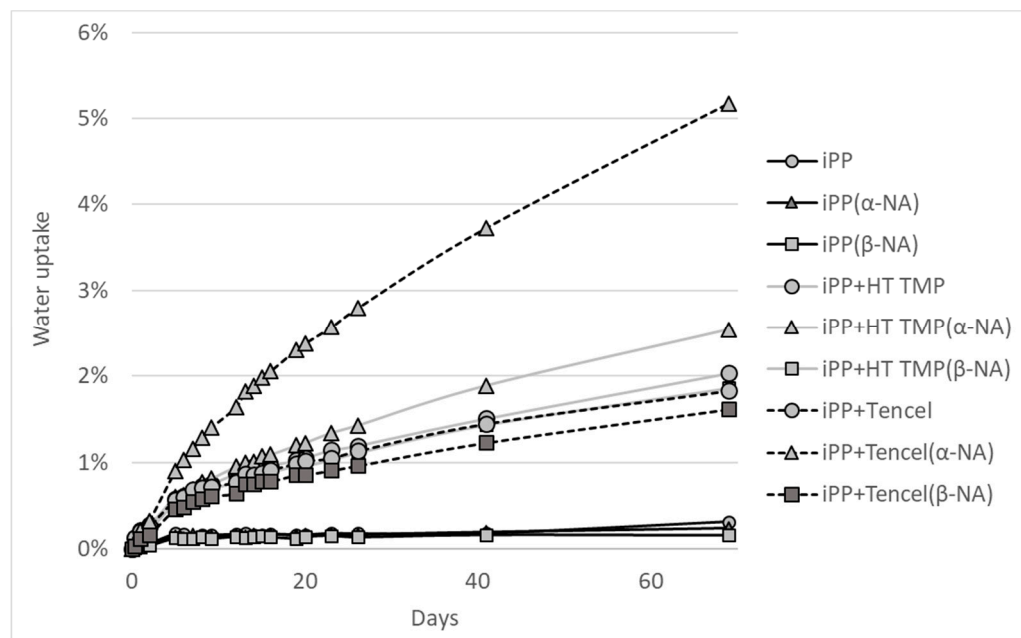


Figure 6. Water uptake of the various iPP composites.

Table 2. Percentage of water uptake of iPP composites after 70 days ($n = 3$, different letters indicate significant difference at $\alpha = 0.05$).

Treatment	Avg	Stdev	Anova
iPP no NA	0.3%	0.1%	A
iPP (α -NA)	0.2%	0.0%	A
iPP (β -NA)	0.2%	0.0%	B
iPP/ HT TMP (no NA)	2.0%	0.0%	C
iPP/ HT TMP (α -NA)	2.5%	0.0%	D
iPP/ HT TMP (β -NA)	1.9%	0.1%	E
iPP/Tencel TM (no NA)	1.8%	0.0%	E
iPP/Tencel TM (α -NA)	5.2%	0.1%	F
iPP/Tencel TM (β -NA)	1.6%	0.0%	G

4. Discussion

The main aim of this study was to improve the mechanical properties of HT TMP composites. We developed an original approach by directly adding the NA on the fibres which could be adopted to tailor the lignocellulosic fibre composite characteristics without an additive incorporation step. The sizing of the fibres was successful; however, the hoped-for tensile strength (α -NA) and impact resistance (β -NA) improvements were not observed. Our strategy failed to improve the mechanical properties of the composite. It may be that the interface between lignocellulosic material and polyolefin matrix in presence of MAPP is already sufficiently strong and is not improved by the TC and nucleation

of the matrix [77]. The absence of covalent linkage between the NA and the fibre might be one of the reasons for the lack of mechanical properties improvement. Another reason could be that the concentration of β -NA is too high. To allow for losses in the blending process, a relatively high concentration of NA was applied. However, losses were modest and nitrogen analysis revealed the concentration of β -NA in the final composite to be 0.4%. Other studies have reported an optimal concentration of β -NA is 0.1%. This allows a maximal growth of β -spherulite in needle like structure and a concentration as low as 0.2% would lead to β -crystals growth competition leading to incomplete spherulite and a decrease on impact strength [78]. When a composite has a high concentration of β -NA, the ordered structure effect cannot be reached [79]. Another aspect could be that the crystal structure at proximity of natural fibre might impair the MAPP efficiently grafting onto the fibre.

5. Conclusions

This study investigated the effect of coating lignocellulosic fibres with NA on the mechanical properties of the resulting iPP-fibre composite. The influence on the TC layer, crystal morphology and proportion, crystallisation temperature, mechanical properties, surface fracture and water uptake were investigated. The addition of NA led to slight increases in composite crystallinity as well as an increase in temperature of crystallisation. The presence of the NA also leads to a significant decrease in crystal size. Sizing the fibres with NA was shown to be an effective method to manipulate the crystallinity of the natural fibre composite. The presence of NA is deeply modifying the nature of matrix crystallinity and its thermal characteristics. However, under the experimental conditions of this study, the mechanical properties of the iPP-fibre composites were mainly influenced by the characteristics of the fibres while the NA had little influence. This suggests that the NAs probably have little influence on interfacial adhesion. In summary:

- The α - and β -NA as fibre sizings have the expected effect on iPP crystals.
- The α - and β -NA cause transcrystallinity at the interphase fibre-matrix in a sandwich composite.
- The α - and β -NA affects the whole matrix crystallinity after compounding.
- The tensile strength and impact strength of the fibre-iPP composite is not significantly improved by the NA.

Author Contributions: Conceptualization, A.T., A.D., R.R. and M.S.; methodology, A.T., A.D. and M.S.; formal analysis, A.T., and R.R.; resources, M.S.; data curation, A.T., and M.S.; writing—original draft preparation, M.S.; writing—review and editing, A.T. and A.D.; visualization, R.R. and A.T.; supervision, M.S.; project administration, M.S. All authors have read and agreed to the published version of the manuscript.

Funding: The New Zealand Ministry of Business, Innovation and Employment (MBIE) funding of Scion supported this work. Scion core funding C04X1703 Scion Platforms Plan (Strategic Science Investment Fund) has been used for this article.

Acknowledgments: We wish to thank Damien Even, Marc Gaugler, Kate Parker, Jeremy Warnes, Doug Gaunt and Elspeth MacRae for their helpful suggestions.

Conflicts of Interest: The authors declare no conflict of interest. The funders had no role in the design of the study; in the collection, analyses, or interpretation of data; in the writing of the manuscript, or in the decision to publish the results.

References

1. Clements, A.; Dunn, M.; Firth, V.; Hubbard, L.; Laonby, J.; Waddington, D. The essential chemical industry. *Chem. Ind. Educ. Cent. Univ. York. UK* **2010**, *511*, 34.
2. Zhang, L.; Qin, Y.; Zheng, G.; Dai, K.; Liu, C.; Yan, X.; Guo, J.; Shen, C.; Guo, Z. Interfacial crystallization and mechanical property of isotactic polypropylene based single-polymer composites. *Polymer* **2016**, *90*, 18–25. [[CrossRef](#)]
3. Li, M.; Li, G.; Zhang, Z.; Dai, X.; Mai, K. Enhanced β -crystallization in polypropylene random copolymer with a supported β -nucleating agent. *Thermochim. Acta* **2014**, *598*, 36–44. [[CrossRef](#)]

4. Kersch, M.; Schmidt, H.-W.; Altstädt, V. Influence of different beta-nucleating agents on the morphology of isotactic polypropylene and their toughening effectiveness. *Polymer* **2016**, *98*, 320–326. [[CrossRef](#)]
5. Zhang, Y.; Zhang, L.; Liu, H.; Du, H.; Zhang, J.; Wang, T.; Zhang, X. Novel approach to tune mechanics of β -nucleation agent nucleated polypropylene: Role of oriented β spherulite. *Polymer* **2013**, *54*, 6026–6035. [[CrossRef](#)]
6. Silvestre, C.; Cimmino, S.; Duraccio, D.; Schick, C. Isothermal crystallization of isotactic poly (propylene) studied by superfast calorimetry. *Macromol. Rapid Commun.* **2007**, *28*, 875–881. [[CrossRef](#)]
7. De Santis, F.; Adamovsky, S.; Titomanlio, G.; Schick, C. Isothermal nanocalorimetry of isotactic polypropylene. *Macromolecules* **2007**, *40*, 9026–9031. [[CrossRef](#)]
8. Grein, C. Toughness of neat, rubber modified and filled β -nucleated polypropylene: From fundamentals to applications. In *Intrinsic Molecular Mobility and Toughness of Polymers ii*; Springer: Berlin/Heidelberg, Germany, 2005; pp. 43–104.
9. Cai, Z.; Zhang, Y.; Li, J.; Xue, F.; Shang, Y.; He, X.; Feng, J.; Wu, Z.; Jiang, S. Real time synchrotron sachs and waxes investigations on temperature related deformation and transitions of β -iPP with uniaxial stretching. *Polymer* **2012**, *53*, 1593–1601. [[CrossRef](#)]
10. Chen, Y.; Wu, Z.; Fan, Q.; Yang, S.; Song, E.; Zhang, Q. Great toughness reinforcement of isotactic polypropylene/elastomer blends with quasi-cocontinuous phase morphology by traces of β -nucleating agents and carbon nanotubes. *Compos. Sci. Technol.* **2018**, *167*, 277–284. [[CrossRef](#)]
11. Shangguan, Y.; Song, Y.; Peng, M.; Li, B.; Zheng, Q. Formation of β -crystal from nonisothermal crystallization of compression-molded isotactic polypropylene melt. *Eur. Polym. J.* **2005**, *41*, 1766–1771. [[CrossRef](#)]
12. Zhang, B.; Chen, J.; Ji, F.; Zhang, X.; Zheng, G.; Shen, C. Effects of melt structure on shear-induced β -cylindrites of isotactic polypropylene. *Polymer* **2012**, *53*, 1791–1800. [[CrossRef](#)]
13. Sun, X.; Li, H.; Zhang, X.; Wang, D.; Yan, S. Effect of fiber molecular weight on the interfacial morphology of iPP fiber/matrix single polymer composites. *Macromolecules* **2006**, *39*, 1087–1092. [[CrossRef](#)]
14. Wang, L.; Yang, M.-B. Unusual hierarchical distribution of β -crystals and improved mechanical properties of injection-molded bars of isotactic polypropylene. *Rsc Adv.* **2014**, *4*, 25135–25147. [[CrossRef](#)]
15. Kang, J.; Wang, B.; Peng, H.; Li, J.; Chen, J.; Gai, J.; Cao, Y.; Li, H.; Yang, F.; Xiang, M. Investigation on the dynamic crystallization and melting behavior of β -nucleated isotactic polypropylene with different stereo-defect distribution—The role of dual-selective β -nucleation agent. *Polym. Adv. Technol.* **2014**, *25*, 97–107. [[CrossRef](#)]
16. Assouline, E.; Pohl, S.; Fulchiron, R.; Gerard, J.-F.; Lustiger, A.; Wagner, H.; Marom, G. The kinetics of α and β transcrystallization in fibre-reinforced polypropylene. *Polymer* **2000**, *41*, 7843–7854. [[CrossRef](#)]
17. Sanadi, A.; Young, R.; Clemons, C.; Rowell, R. Recycled newspaper fibers as reinforcing fillers in thermoplastics: Part i-analysis of tensile and impact properties in polypropylene. *J. Reinf. Plast. Compos.* **1994**, *13*, 54–67. [[CrossRef](#)]
18. Thomason, J. The influence of fibre length and concentration on the properties of glass fibre reinforced polypropylene: 5. Injection moulded long and short fibre PP. *Compos. Part A Appl. Sci. Manuf.* **2002**, *33*, 1641–1652. [[CrossRef](#)]
19. Hyer, M.W. *Stress Analysis of Fiber-Reinforced Composite Materials*; DEStech Publications, Inc.: Lancaster, PA, USA, 2009.
20. Bourmaud, A.; Ausias, G.; Lebrun, G.; Tachon, M.L.; Baley, C. Observation of the structure of a composite polypropylene/flax and damage mechanisms under stress. *Ind. Crop. Prod.* **2013**, *43*, 225–236. [[CrossRef](#)]
21. Thomason, J.; Van Rooyen, A. Transcrysallized interphase in thermoplastic composites. *J. Mater. Sci.* **1992**, *27*, 897–907. [[CrossRef](#)]
22. Quan, H.; Li, Z.-M.; Yang, M.-B.; Huang, R. On transcrystallinity in semi-crystalline polymer composites. *Compos. Sci. Technol.* **2005**, *65*, 999–1021. [[CrossRef](#)]
23. Yan, B.; Wu, H.; Jiang, G.; Guo, S.; Huang, J. Interfacial crystalline structures in injection over-molded polypropylene and bond strength. *Acs Appl. Mater. Interfaces* **2010**, *2*, 3023–3036. [[CrossRef](#)] [[PubMed](#)]
24. Xu, H.; Xie, L.; Jiang, X.; Li, X.-J.; Li, Y.; Zhang, Z.-J.; Zhong, G.-J.; Li, Z.-M. Toward stronger transcrystalline layers in poly(l-lactic acid)/natural fiber biocomposites with the aid of an accelerator of chain mobility. *J. Phys. Chem. B* **2014**, *118*, 812–823. [[CrossRef](#)] [[PubMed](#)]
25. Garkhail, S.; Wieland, B.; George, J.; Soyeabkaew, N.; Peijs, T. Transcrysallisation in PP/flax composites and its effect on interfacial and mechanical properties. *J. Mater. Sci.* **2009**, *44*, 510–519. [[CrossRef](#)]

26. Borysiak, S. Fundamental studies on lignocellulose/polypropylene composites: Effects of wood treatment on the transcrystalline morphology and mechanical properties. *J. Appl. Polym. Sci.* **2013**, *127*, 1309–1322. [[CrossRef](#)]
27. Wang, C.; Liu, F.-H.; Huang, W.-H. Electrospun-fiber induced transcrystallization of isotactic polypropylene matrix. *Polymer* **2011**, *52*, 1326–1336. [[CrossRef](#)]
28. Ning, N.; Zhang, W.; Yan, J.; Xu, F.; Wang, T.; Su, H.; Tang, C.; Fu, Q. Largely enhanced crystallization of semi-crystalline polymer on the surface of glass fiber by using graphene oxide as a modifier. *Polymer* **2013**, *54*, 303–309. [[CrossRef](#)]
29. Wang, Y.; Tong, B.; Hou, S.; Li, M.; Shen, C. Transcrystallization behavior at the poly (lactic acid)/sisal fibre biocomposite interface. *Compos. Part A: Appl. Sci. Manuf.* **2011**, *42*, 66–74. [[CrossRef](#)]
30. Sorieul, M.; Dickson, A.; Hill, S.J.; Pearson, H. Plant fibre: Molecular structure and biomechanical properties, of a complex living material, influencing its deconstruction towards a biobased composite. *Materials* **2016**, *9*, 618. [[CrossRef](#)]
31. Markiewicz, E.; Borysiak, S.; Paukszata, D. Polypropylene-lignocellulosic material composites as promising sound absorbing materials. *Polimery* **2009**, *54*, 430–435. [[CrossRef](#)]
32. Saheb, D.N.; Jog, J.P. Natural fiber polymer composites: A review. *Adv. Polym. Technol. J. Polym. Process. Inst.* **1999**, *18*, 351–363. [[CrossRef](#)]
33. Karimi, K.; Taherzadeh, M.J. A critical review of analytical methods in pretreatment of lignocelluloses: Composition, imaging, and crystallinity. *Bioresour. Technol.* **2016**, *200*, 1008–1018. [[CrossRef](#)] [[PubMed](#)]
34. Donaldson, L.; Lomax, T.D. Adhesive/fibre interaction in medium density fibreboard. *Wood Sci. Technol.* **1989**, *23*, 371–380. [[CrossRef](#)]
35. Shao, Z.; Li, K. The effect of fiber surface lignin on interfiber bonding. *J. Wood Chem. Technol.* **2006**, *26*, 231–244. [[CrossRef](#)]
36. Warnes, J.M.; Fernyhough, A.; Anderson, C.R.; Lee, B.J.; Witt, M.R.J. Method for Producing Wood Fibre Pellets. U.S. Patent 9,511,508, 6 December 2016.
37. Thumm, A.; Even, D.; Gini, P.-Y.; Sorieul, M. Processing and properties of mdf fibre-reinforced biopolymers with chain extender additives. *Int. J. Polym. Sci.* **2018**, *2018*, 9601753. [[CrossRef](#)]
38. Bourban, C.; Karamuk, E.; De Fondaumiere, M.; Ruffieux, K.; Mayer, J.; Wintermantel, E. Processing and characterization of a new biodegradable composite made of a phb/v matrix and regenerated cellulosic fibers. *J. Environ. Polym. Degrad.* **1997**, *5*, 159–166.
39. Graupner, N.; Müssig, J. A comparison of the mechanical characteristics of kenaf and lyocell fibre reinforced poly (lactic acid)(pla) and poly (3-hydroxybutyrate)(phb) composites. *Compos. Part A Appl. Sci. Manuf.* **2011**, *42*, 2010–2019. [[CrossRef](#)]
40. McDonald, A.; Clare, A.; Dawson, B. Surface characterisation of radiata pine high-temperature TMP fibres by x-ray photo-electron spectroscopy. In Proceedings of the 53rd General APPITA Conference, Rotorua, New Zealand, 19–23 April 1999; pp. 51–57.
41. Dickson, A.; Teuber, L.; Gaugler, M.; Sandquist, D. Effect of processing conditions on wood and glass fiber length attrition during twin screw composite compounding. *J. Appl. Polym. Sci.* **2020**, *137*, 48551. [[CrossRef](#)]
42. Wolters, W.S.; Hanssen, R.; Palanisami, T.K.; Dotson, D.L. Nucleating Agent Additive Compositions and Methods. U.S. Patent 7,659,336, 9 February 2010.
43. Ye, J.; Fang, J.; Zhang, L.; Li, C. Transcrystalline induced by mwcnts and organic nucleating agents at the interface of glass fiber/polypropylene. *Polym. Compos.* **2018**, *39*, 3424–3433. [[CrossRef](#)]
44. Bassett, D.C.; Olley, R.H. On the lamellar morphology of isotactic polypropylene spherulites. *Polymer* **1984**, *25*, 935–943. [[CrossRef](#)]
45. Schindelin, J.; Arganda-Carreras, I.; Frise, E.; Kaynig, V.; Longair, M.; Pietzsch, T.; Preibisch, S.; Rueden, C.; Saalfeld, S.; Schmid, B.; et al. Fiji: An open-source platform for biological-image analysis. *Nat. Methods* **2012**, *9*, 676. [[CrossRef](#)]
46. Blaine, R.L. Thermal applications note. *Polym. Heats Fusion*, 2002.
47. Ljungberg, N.; Cavaillé, J.-Y.; Heux, L. Nanocomposites of isotactic polypropylene reinforced with rod-like cellulose whiskers. *Polymer* **2006**, *47*, 6285–6292. [[CrossRef](#)]
48. Habibi, Y.; Dufresne, A. Highly filled bionanocomposites from functionalized polysaccharide nanocrystals. *Biomacromolecules* **2008**, *9*, 1974–1980. [[CrossRef](#)] [[PubMed](#)]

49. Gray, D.G. Transcristallization of polypropylene at cellulose nanocrystal surfaces. *Cellulose* **2008**, *15*, 297–301. [[CrossRef](#)]
50. Nwabunma, D.; Kyu, T. *Polyolefin Composites*; John Wiley & Sons: Hoboken, NJ, USA, 2008.
51. Gray, D.G. Polypropylene transcristallization at the surface of cellulose fibers. *J. Polym. Sci. Polym. Lett. Ed.* **1974**, *12*, 509–515. [[CrossRef](#)]
52. Kłapiszewski, Ł.; Grząbka-Zasadzińska, A.; Borysiak, S.; Jasionowski, T. Preparation and characterization of polypropylene composites reinforced by functional zno/lignin hybrid materials. *Polym. Test.* **2019**, *79*, 106058. [[CrossRef](#)]
53. Wunderlich, B.; Grebowicz, J. Thermotropic mesophases and mesophase transitions of linear, flexible macromolecules. In *Liquid Crystal Polymers ii/iii*; Springer: Berlin/Heidelberg, Germany, 1984; pp. 1–59.
54. Paukszta, D.; Borysiak, S. The influence of processing and the polymorphism of lignocellulosic fillers on the structure and properties of composite materials—A review. *Materials* **2013**, *6*, 2747–2767. [[CrossRef](#)]
55. Borysiak, S. Influence of wood mercerization on the crystallization of polypropylene in wood/PP composites. *J. Therm. Anal. Calorim.* **2012**, *109*, 595–603. [[CrossRef](#)]
56. Borysiak, S.; Doczekalska, B. The influence of chemical modification of wood on its nucleation ability in polypropylene composites. *Polimery* **2009**, *54*, 820–827. [[CrossRef](#)]
57. Dong, M.; Guo, Z.; Su, Z.; Yu, J. The effects of crystallization condition on the microstructure and thermal stability of isotactic polypropylene nucleated by β -form nucleating agent. *J. Appl. Polym. Sci.* **2011**, *119*, 1374–1382. [[CrossRef](#)]
58. Khan, M.; Afaq, S.K.; Khan, N.U.; Ahmad, S. Cycle time reduction in injection molding process by selection of robust cooling channel design. *Isrn Mech. Eng.* **2014**, *2014*, 1–8. [[CrossRef](#)]
59. Firgo, H.; Schuster, K.; Suchomel, F.; Männer, J.; Burrow, T.; Abu Rous, M. The functional properties of tencel®—a current update. *Lenzing. Ber.* **2006**, *85*, 22–30.
60. Bera, M.; Alagirusamy, R.; Das, A. A study on interfacial properties of jute-PP composites. *J. Reinf. Plast. Compos.* **2010**, *29*, 3155–3161. [[CrossRef](#)]
61. Sun, X.; Li, H.; Wang, J.; Yan, S. Shear-induced interfacial structure of isotactic polypropylene (iPP) in iPP/fiber composites. *Macromolecules* **2006**, *39*, 8720–8726. [[CrossRef](#)]
62. Canetti, M.; De Chirico, A.; Audisio, G. Morphology, crystallization and melting properties of isotactic polypropylene blended with lignin. *J. Appl. Polym. Sci.* **2004**, *91*, 1435–1442. [[CrossRef](#)]
63. Zhang, Z.; Wang, C.; Yang, Z.; Chen, C.; Mai, K. Crystallization behavior and melting characteristics of PP nucleated by a novel supported β -nucleating agent. *Polymer* **2008**, *49*, 5137–5145. [[CrossRef](#)]
64. Raka, L.; Bogoeva-Gaceva, G. Crystallization of polypropylene: Application of differential scanning calorimetry part ii. Crystal forms and nucleation. *Contrib. Sect. Nat. Math. Biotech. Sci.* **2017**, *8*:29, 1–2. [[CrossRef](#)]
65. Ou, R.; Xie, Y.; Wolcott, M.P.; Sui, S.; Wang, Q. Morphology, mechanical properties, and dimensional stability of wood particle/high density polyethylene composites: Effect of removal of wood cell wall composition. *Mater. Des.* **2014**, *58*, 339–345. [[CrossRef](#)]
66. Arbelaitz, A.; Cantero, G.; Fernandez, B.; Mondragon, I.; Ganan, P.; Kenny, J. Flax fiber surface modifications: Effects on fiber physico mechanical and flax/polypropylene interface properties. *Polym. Compos.* **2005**, *26*, 324–332. [[CrossRef](#)]
67. Graupner, N.; Fischer, H.; Ziegmann, G.; Müssig, J. Improvement and analysis of fibre/matrix adhesion of regenerated cellulose fibre reinforced PP-, MAPP-and PLA-composites by the use of eucalyptus globulus lignin. *Compos. Part B Eng.* **2014**, *66*, 117–125. [[CrossRef](#)]
68. Peltola, H.; Pääkkönen, E.; Jetsu, P.; Heinemann, S. Wood based pla and PP composites: Effect of fibre type and matrix polymer on fibre morphology, dispersion and composite properties. *Compos. Part A Appl. Sci. Manuf.* **2014**, *61*, 13–22. [[CrossRef](#)]
69. Peltola, H.; Immonen, K.; Johansson, L.S.; Virkajarvi, J.; Sandquist, D. Influence of pulp bleaching and compatibilizer selection on performance of pulp fiber reinforced pla biocomposites. *J. Appl. Polym. Sci.* **2019**, *136*, 47955. [[CrossRef](#)]
70. Bahia, H.S. Process of Making Lyocell Fibre or Film. U.S. Patent 6,258,304, 10 July 2001.
71. Solala, I.; Antikainen, T.; Reza, M.; Johansson, L.-S.; Hughes, M.; Vuorinen, T. Spruce fiber properties after high-temperature thermomechanical pulping (HT-TMP). *Holzforschung* **2014**, *68*, 195–201. [[CrossRef](#)]

72. Panthapulakkal, S.; Sain, M. Injection-molded short hemp fiber/glass fiber-reinforced polypropylene hybrid composites—Mechanical, water absorption and thermal properties. *J. Appl. Polym. Sci.* **2007**, *103*, 2432–2441. [[CrossRef](#)]
73. Ayrilmis, N.; Kaymakci, A.; Ozdemir, F. Physical, mechanical, and thermal properties of polypropylene composites filled with walnut shell flour. *J. Ind. Eng. Chem.* **2013**, *19*, 908–914. [[CrossRef](#)]
74. Arbelaitz, A.; Fernandez, B.; Ramos, J.; Retegi, A.; Llano-Ponte, R.; Mondragon, I. Mechanical properties of short flax fibre bundle/polypropylene composites: Influence of matrix/fibre modification, fibre content, water uptake and recycling. *Compos. Sci. Technol.* **2005**, *65*, 1582–1592. [[CrossRef](#)]
75. Sreekala, M.; Thomas, S. Effect of fibre surface modification on water-sorption characteristics of oil palm fibres. *Compos. Sci. Technol.* **2003**, *63*, 861–869. [[CrossRef](#)]
76. Wu, C.-M.; Lai, W.-Y.; Wang, C.-Y. Effects of surface modification on the mechanical properties of flax/ β -polypropylene composites. *Materials* **2016**, *9*, 314. [[CrossRef](#)]
77. Dickson, A.R.; Even, D.; Warnes, J.M.; Fernyhough, A. The effect of reprocessing on the mechanical properties of polypropylene reinforced with wood pulp, flax or glass fibre. *Compos. Part A: Appl. Sci. Manuf.* **2014**, *61*, 258–267. [[CrossRef](#)]
78. Sheng, Q.; Zhang, Y.; Xia, C.; Mi, D.; Xu, X.; Wang, T.; Zhang, J. A new insight into the effect of β modification on the mechanical properties of iPP: The role of crystalline morphology. *Mater. Des.* **2016**, *95*, 247–255. [[CrossRef](#)]
79. Kang, J.; Weng, G.; Chen, Z.; Chen, J.; Cao, Y.; Yang, F.; Xiang, M. New understanding in the influence of melt structure and β -nucleating agents on the polymorphic behavior of isotactic polypropylene. *Rsc Adv.* **2014**, *4*, 29514–29526. [[CrossRef](#)]



© 2020 by the authors. Licensee MDPI, Basel, Switzerland. This article is an open access article distributed under the terms and conditions of the Creative Commons Attribution (CC BY) license (<http://creativecommons.org/licenses/by/4.0/>).